

RESEARCH ARTICLE

10.1002/2017JB014095

Key Points:

- A high-spin to low-spin transition of octahedral Fe³⁺ in Fe-bearing CF phase is observed at 25–35 GPa
- Spin transition of Fe³⁺ in Al-rich phases results in elastic softening of subducted MORB
- Elastic anomalies due to spin transition should be taken into account to understand seismic signatures in the lower mantle

Supporting Information:

- Supporting Information S1

Correspondence to:

X. Wu,
wuxiang@cug.edu.cn

Citation:

Wu, Y., F. Qin, X. Wu, H. Huang, C. A. McCammon, T. Yoshino, S. Zhai, Y. Xiao, and V. B. Prakapenka (2017), Spin transition of ferric iron in the calcium-ferrite type aluminous phase, *J. Geophys. Res. Solid Earth*, 122, 5935–5944, doi:10.1002/2017JB014095.







Received 13 FEB 2017

Accepted 14 JUL 2017

Accepted article online 18 JUL 2017

Published online 1 AUG 2017

Spin transition of ferric iron in the calcium-ferrite type aluminous phase

Ye Wu¹ , Fei Qin², Xiang Wu³ , Haijun Huang¹, Catherine A. McCammon⁴ , Takashi Yoshino⁵ , Shuangmeng Zhai⁶ , Yuming Xiao⁷, and Vitali B. Prakapenka⁸ 

¹School of Science, Wuhan University of Technology, Wuhan, China, ²Key Laboratory of Orogenic Belts and Crustal Evolution, MOE, and School of Earth and Space Sciences, Peking University, Beijing, China, ³State Key Laboratory of Geological Processes and Mineral Resources, China University of Geosciences, Wuhan, China, ⁴Bayerisches Geoinstitut, Universität Bayreuth, Bayreuth, Germany, ⁵Institute for Planetary Materials, Okayama University, Misasa, Japan, ⁶Key Laboratory of High-temperature and High-pressure Study of the Earth's Interior, Institute of Geochemistry, Chinese Academy of Sciences, Guiyang, China, ⁷HPCAT, Geophysical Laboratory, Carnegie Institution of Washington, Argonne, Illinois, USA, ⁸GeoSoilEnviroCARS, University of Chicago, Chicago, Illinois, USA

Abstract We investigated Fe-free and Fe-bearing CF phases using nuclear forward scattering and X-ray diffraction coupled with diamond anvil cells up to 80 GPa at room temperature. Octahedral Fe³⁺ ions in the Fe-bearing CF phase undergo a high-spin to low-spin transition at 25–35 GPa, accompanied by a volume reduction of ~2.0% and a softening of bulk sound velocity up to 17.6%. Based on the results of this study and our previous studies, both the NAL and CF phases, which account for 10–30 vol % of subducted MORB in the lower mantle, are predicted to undergo a spin transition of octahedral Fe³⁺ at lower mantle pressures. Spin transitions in these two aluminous phases result in an increase of density of 0.24% and a pronounced softening of bulk sound velocity up to 2.3% for subducted MORB at 25–60 GPa and 300 K. The anomalous elasticity region expands and moves to 30–75 GPa at 1200 K and the maximum of the V_{ϕ} reduction decreases to ~1.8%. This anomalous elastic behavior of Fe-bearing aluminous phases across spin transition zones may be relevant in understanding the observed seismic signatures in the lower mantle.

1. Introduction

Since the deep subduction of slabs leads to chemical heterogeneity of the mantle, it is important to study the fate of subducted slabs to understand geodynamic processes and chemical evolution of the Earth. Both seismic tomography studies and high-pressure (HP) high-temperature (HT) experimental simulations have indicated that subducted slabs can penetrate into the mantle. There is both stagnation near the 660 km discontinuity, and also accumulation at the bottom of the lower mantle [Fukao and Obayashi, 2013; Hirose et al., 2005; Ricolleau et al., 2010; Zhao, 2004]. Subducted slabs have higher seismic wave velocities than peridotite in the Earth's mantle due to their different temperatures and chemical compositions [Bina and Helffrich, 2014; Fukao et al., 2009]. Seismic signatures, such as scatterers and discontinuities observed in the lower mantle, are proposed to be related to subducted basalt [Castle and van der Hilst, 2003; Kaneshima, 2013; Korenaga, 2015; Niu, 2014; Vinnik et al., 2001].

As a rock representative of subducted ocean crust, mid-ocean ridge basalt (MORB) is enriched in aluminum but depleted in magnesium compared with mantle peridotite [Green et al., 1979; Sun, 1982]. The high Al₂O₃ content (~16 wt %) in MORB composition stabilizes Al-rich phases, specifically the new hexagonal aluminous phase (NAL, $P6_3/m$) and calcium-ferrite type phase (CF, $Pbnm$) in the lower mantle [Irifune and Ringwood, 1993; Miyajima et al., 1999; Yamada et al., 1983]. These two phases account for 10–30 vol % of subducted basalt in the lower mantle. Both the NAL and CF phases coexist at pressures of 25–50 GPa, but only the CF phase is stable at pressures higher than 50 GPa [Ricolleau et al., 2010]. Additionally, the NAL phase has been found to transform to the CF phase at HP-HT conditions in the NaAlSiO₄-MgAl₂O₄ system [Imada et al., 2011; Ono et al., 2009].

Iron is the most abundant 3d transition metal element in the Earth's mantle and has multiple valence (Fe²⁺ and Fe³⁺) and spin states (HS: high spin; LS: low spin), which significantly affect elastic properties of the hosts at HP-HT conditions [Lin et al., 2013]. A HS-to-LS transition of octahedral Fe³⁺ in the Fe-bearing NAL phase has been recently observed at approximately 30 GPa [Lobanov et al., 2017; Wu et al., 2016a]. Correspondingly, the Fe-bearing NAL phase displays a volume reduction of 1.0% (~1.2 Å³) in the spin transition zone. The Fe³⁺ spin

transition results in elastic softening of the bulk modulus (up to 17.6%) and the bulk sound velocity (up to 9.4%). These distinct elastic properties of the Fe-bearing NAL phase may contribute to observed seismic heterogeneities around subducted slabs at depths of 660–1200 km [Kaneshima, 2013; Niu *et al.*, 2003; Wu *et al.*, 2016a]. Additionally, based on our studies of single-crystal elasticity of the NAL phase at high pressure, the NAL phase exhibits high-velocity anisotropies and may be a potential source of seismic anisotropy in the lower mantle [Wu *et al.*, 2016b].

As another important Al-rich phase, the CF phase with ~10 vol % in subducted MORB is stable within the entire lower mantle, and the CF phase hosts 12–35 mol % iron in the lower mantle (Table S2 in the supporting information). To further elucidate the geophysical implications of Al-rich phases during the subduction process, we have investigated Fe-free and Fe-bearing CF phases using nuclear forward scattering (NFS) and single-crystal X-ray diffraction (XRD) coupled with diamond anvil cells (DACs). A HS-to-LS transition of octahedral Fe³⁺ in Fe-bearing CF phase is observed at 25–35 GPa and causes an abnormal reduction of lattice parameters. We combine the results of this study with those of our previous study on the NAL phase to model density and bulk sound velocity profiles of subducted MORB and discuss the geophysical implications of Al-rich phases on seismic signatures in the vicinity of subduction zones in the lower mantle.

2. Experiments

Fe-free and Fe-bearing CF phases (RUN #: 5K2124 and 5K2681, respectively) were synthesized at 25 GPa and 1600°C using a 5000t Kawai-type multianvil apparatus. Mixtures of Na₂CO₃, Al₂O₃ (⁵⁷Fe₂O₃, >95% enrichment in ⁵⁷Fe), and SiO₂ in the molar ratio 1:1:2 were sintered at 1200°C for 12 h and then used as starting materials for HP-HT synthesis experiments. XRD patterns showed the recovered samples to be CF phase with space group *Pbnm*. Chemical compositions were determined by electron microprobe analysis using an accelerating voltage of 15 kV and a beam current of 10 nA to minimize the loss of Na (Table S1). Fe-free and Fe-bearing CF phases have chemical compositions Na_{0.93}Al_{1.02}Si_{1.00}O₄ and Na_{0.88}Al_{0.99}Fe_{0.13}Si_{0.94}O₄, respectively. The Fe content of the CF phase in this study is 13 mol %, which is close to the lower bound of iron contents (12–35 mol %) for the CF phase in natural MORB compositions (Table S2). The Fe-bearing sample was additionally examined by conventional Mössbauer spectroscopy. Analysis of the Mössbauer spectrum indicates that approximately 10% of the total iron is Fe²⁺ with quadrupole splitting (QS) of 3.38 mm/s and isomer shift (IS) of 1.22(3) mm/s (relative to α -Fe), with the remaining 90% as Fe³⁺ with QS = 0.94 mm/s and IS = 0.33(1) mm/s (Figure S2).

High-pressure NFS experiments were performed at the High-Pressure Collaborative Access Team (HPCAT) sector of the Advanced Photon Source (APS), Argonne National Laboratory (ANL). An incident X-ray beam with an energy of 14.4125 keV and a resolution of 2.2 meV was used to excite ⁵⁷Fe nuclei in the sample. A two-sided polished single crystal of the Fe-bearing CF phase was loaded into a symmetric-type DAC with a Re gasket. Neon was used as the pressure medium and two ruby spheres were placed next to the crystal for pressure calibration [Mao *et al.*, 1986]. The NFS spectra were analyzed using the CONUSS program to derive hyperfine parameters of iron in the Fe-bearing CF phase [Sturhahn, 2000].

High-pressure XRD experiments were carried out at the GeoSoilEnviroConsortium for Advanced Radiation Sources (GSECARS) sector of the APS using a monochromatic X-ray beam with a wavelength of 0.3344 Å. Two double-sided polished single-crystal platelets, one for the Fe-free CF phase and another for the Fe-bearing CF phase, were loaded into the sample chamber of a Re gasket in a symmetric-type DAC, together with neon as pressure medium. Fine platinum powder was placed next to the samples for pressure calibration [Fei *et al.*, 2007]. Single-crystal diffraction patterns were evaluated to obtain *d* spacing values using the GSE_ADA program [Dera *et al.*, 2013], and lattice parameters were obtained using the UnitCell program [Holland and Redfern, 1997] (Figure S3).

3. Results and Discussion

3.1. Crystal Chemistry of the CF Phase

Chemical compositions of CF phases in MORB compositions from previous studies exhibit complex solid solutions but for simplicity can be considered to be along the join NaAlSiO₄-MgAl₂O₄ with a small amount of Ca, Fe, Cr, and Ti [Funamori *et al.*, 2000; Hirose *et al.*, 1999, 2005; Kesson *et al.*, 1994; Litasov and Ohtani, 2004;

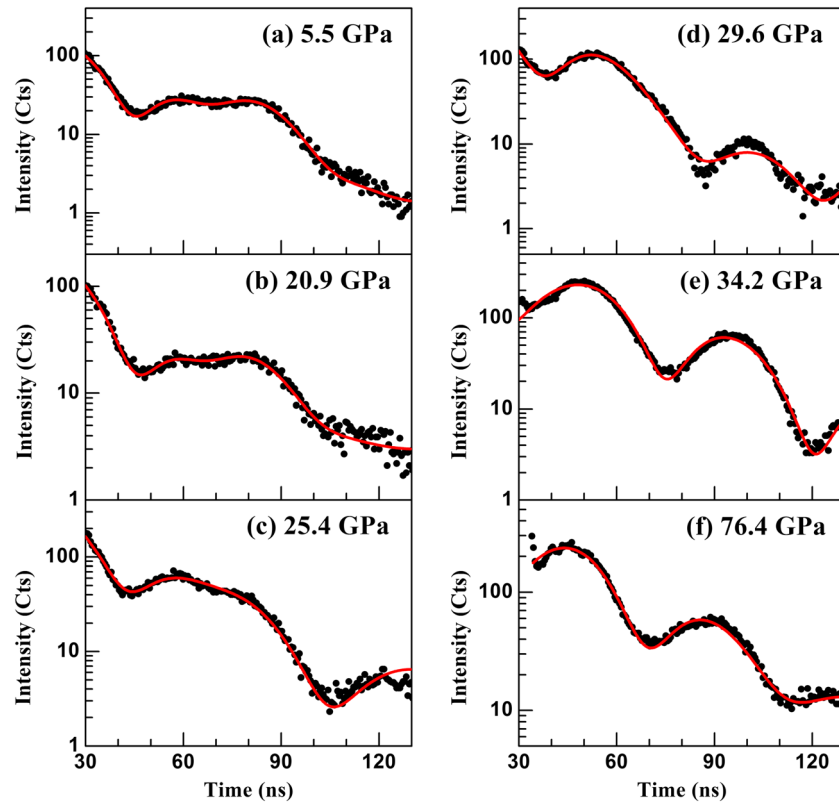
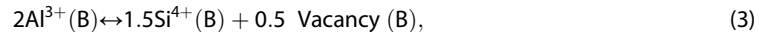
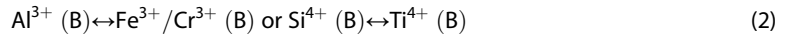
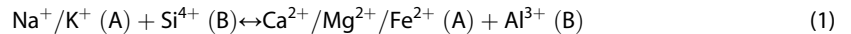


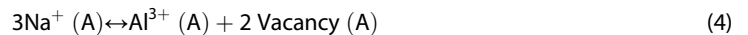
Figure 1. Representative NFS spectra of the Fe-bearing CF phase ($\text{Na}_{0.88}\text{Al}_{0.99}\text{Fe}_{0.13}\text{Si}_{0.94}\text{O}_4$) at high pressures. Spectra at 29.6 and 34.2 GPa were modeled with three doublets, one for Fe^{2+} and two for Fe^{3+} , while the other spectra were modeled with a two-doublet model, one each for Fe^{2+} and Fe^{3+} .

[Miyajima *et al.*, 2001; Ono *et al.*, 2001; Ricolleau *et al.*, 2010] (Table S2). Based on charge balance and cation radius, there are three main substitutions proposed for the ideal CF-type AB_2O_4 (NaAlSiO_4 or MgAl_2O_4):



leading to the composition $[\text{Na}^+, \text{Mg}^{2+}, \text{Ca}^{2+}, \text{Fe}^{2+}]_1[\text{Al}^{3+}, \text{Si}^{4+}, \text{Fe}^{3+}, \text{Cr}^{3+}, \text{Ti}^{4+}]_2\text{O}_4$ in the lower mantle.

Fe-free and Fe-bearing CF phases have chemical compositions of $\text{Na}_{0.93}\text{Al}_{1.02}\text{Si}_{1.00}\text{O}_4$ and $\text{Na}_{0.88}\text{Al}_{0.99}\text{Fe}_{0.13}\text{Si}_{0.94}\text{O}_4$, respectively, based on electron microprobe analysis in this study. We consider the loss of Na to be minimal based on the low electron current and larger beam size (15 kV, 10 nA, and 5 μm diameter). According to the hyperfine parameters determined using MS, Fe^{2+} (10% of total iron) occupies the A site together with Na^+ , and the remaining iron, 90% Fe^{3+} , is located at the octahedral B site along with Al^{3+} and Si^{4+} (Figures S1 and S2). On the basis of four oxygen atoms in the ideal CF phase AB_2O_4 , the cation sums on the B site for Fe-free and Fe-bearing CF phases are 2.023 and 2.048, respectively, while the corresponding cation sums on the A site are 0.931 and 0.891. The cation excess on the B site and cation deficiency on the A site suggests that some of the Al^{3+} may be located at the A site according to the substitution:



The chemical compositions of CF phases in this study are compared with those from basalt compositions in the literature [Walter *et al.*, 2011] (Table S2). Due to the lack of MS measurements, the amount of Fe^{3+} on the B site is calculated as $2 - (\text{Al}^{3+} + \text{Si}^{4+} + \text{Ti}^{4+} + \text{Cr}^{3+})$ or until the total amount of Fe is used. The remaining iron is considered as Fe^{2+} on the A site. Both cation deficiency and excess on the A and B sites exist in CF phases in natural basaltic compositions.

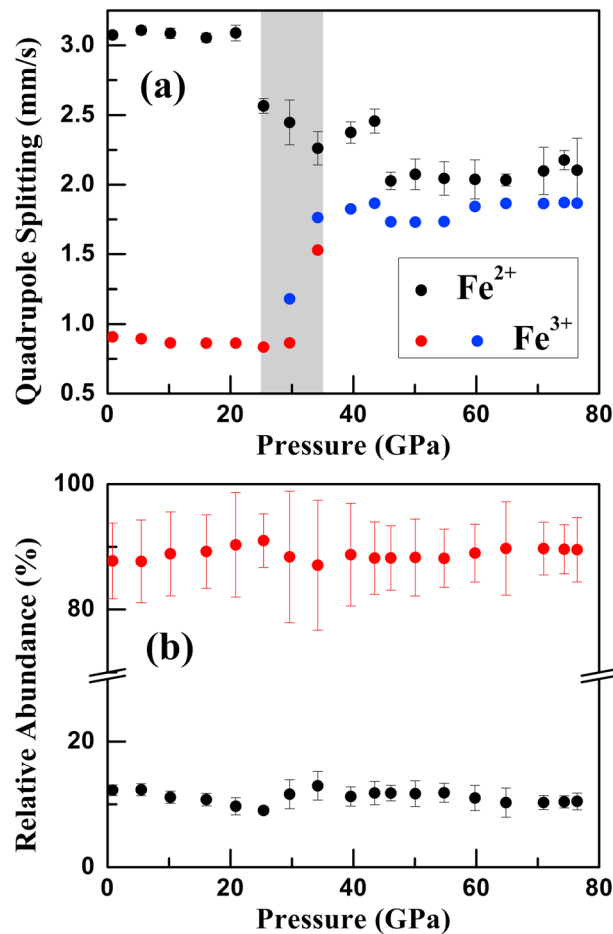


Figure 2. (a) Quadrupole splitting and (b) relative abundance of Fe²⁺ (black dots) and Fe³⁺ (red and blue dots) in the Fe-bearing CF phase at high pressure. The gray shaded region represents the spin transition zone of octahedral Fe³⁺.

spectra are plotted in Figure 1. The NFS spectra at 0.8 GPa can be well fitted using a two-doublet model, one Fe²⁺ (QS = 3.07(3) mm/s and relative abundance (wt) = 12(1) %) and one Fe³⁺ (QS = 0.908(3) mm/s and wt = 88(6) %), which are consistent with results of conventional Mössbauer spectroscopy at ambient conditions (Figure S2 and Table S4). With increasing pressure, the spectrum at 25.4 GPa changes significantly with the appearance of a new quantum beat around 100–110 ns (Figure 1c). The intensity of this new beat increases and the spectra move from long time delayed to short time delayed with increasing pressure. Beyond 35 GPa the spectra show no obvious further change (Figures 1e and 1f). The pressure evolution of the NFS spectra is consistent with a change in the electronic configuration of iron in the Fe-bearing CF phase.

A two-doublet model, one each for Fe²⁺ and Fe³⁺, was used to fit the NFS spectra except for the spectra at 29.6 and 34.2 GPa, which were fitted with a three-doublet model, one for Fe²⁺ and two for Fe³⁺. At pressures below 25 GPa, the doublet of Fe²⁺ with a QS of ~3.0 mm/s is assigned to HS Fe²⁺ and the doublet of Fe³⁺ with a QS of 0.8–0.9 mm/s is assigned to HS Fe³⁺. At 25 < P < 35 GPa, the QS of Fe³⁺ increases from ~0.8 to ~1.8 mm/s, while QS of Fe²⁺ correspondingly decreases from ~3.0 to ~2.3 mm/s (Figure 2a). These results suggest that a HS-to-LS transition of Fe³⁺ occurs in the Fe-bearing CF phase at 25–35 GPa, based on the dramatic increase of QS at an Fe³⁺ spin transition. The decrease of Fe²⁺ QS is likely due to a more symmetric local environment as a result of the spin transition of neighboring Fe³⁺ rather than a HS-to-LS transition of Fe²⁺, since a spin transition typically leads to a very low QS (almost zero). Above 35 GPa, the NFS spectra are well fitted with two doublets of iron, one for HS Fe²⁺ and another for LS Fe³⁺. In addition, the Fe³⁺/ΣFe ratio maintains a constant value of ~90% at high pressure up to 76 GPa (Figure 2b).

We note that our samples are Mg deficient compared with the expected CF phase in the lower mantle. Such cation substitutions likely do not have a significant effect on the physical properties of the CF phase such as density. Zero-pressure densities of CF phases with different compositions are summarized in Table S3, including the end-members CaAl₂O₄ (~3.98 g/cm³) [Akaogi et al., 1999], MgAl₂O₄ (~3.94 g/cm³) [Kojitani et al., 2007; Sueda et al., 2009], and NaAlSiO₄ (3.88–3.92 g/cm³) [Dubrovinsky et al., 2002; Guignot and Andrault, 2004; Yamada et al., 1983], Fe-free and Fe-bearing NaAlSiO₄-MgAl₂O₄ solid solutions (3.81–4.01 g/cm³) [Funamori et al., 2000; Imada et al., 2012; Litasov and Ohtani, 2004; Ono et al., 2001]. The variation of density with composition is small and even the end-members MgAl₂O₄ and NaAlSiO₄ have similar densities. The densities of Fe-free and Fe-bearing CF phases in this study are 3.88 and 3.96 g/cm³, respectively, which are in good agreement with results from previous experiments on basaltic compositions.

3.2. Spin Transition of Fe³⁺ in the CF Phase

NFS spectra of the Fe-bearing CF phase were collected up to 76 GPa at room temperature. Several representative

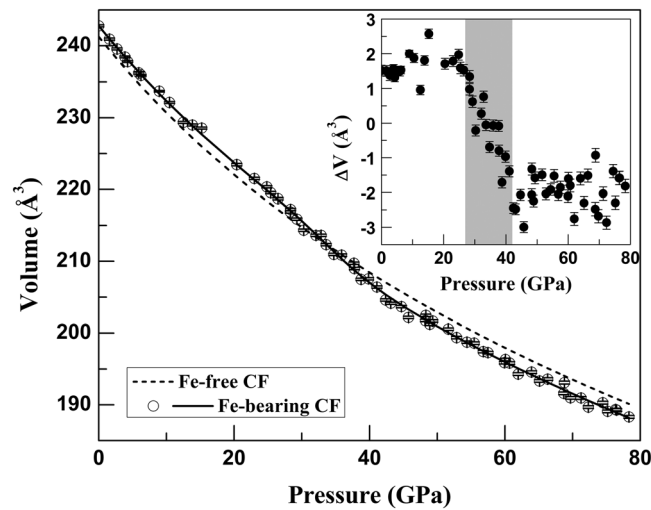


Figure 3. Unit-cell volumes of the CF phase at high pressures. The figure inset shows the volume difference (ΔV) between Fe-bearing and Fe-free CF phases. Open circles: experimental data; solid and dashed lines: modeled results using B-M EoS and the method from *Wentzcovitch et al.* [2009]. The gray shaded region represents the spin transition zone of octahedral Fe^{3+} .

and the end pressure for the HS state (P_{HS}), the volume differences (ΔV) between Fe-bearing and Fe-free CF phases were calculated, yielding $P_{\text{LS}} = 27$ GPa and $P_{\text{HS}} = 42$ GPa with a width of 15 GPa (Figure 3 inset). The pressure region of the Fe^{3+} spin transition determined from XRD (27–42 GPa) is larger than that from NFS analysis (25–35 GPa). This difference is not unreasonable and may be due to different sensitivities of the techniques. NFS is sensitive to the local environment of iron atoms, while XRD monitors long-range changes.

The pressure-volume (P - V) data of both Fe-free and Fe-bearing CF phases are fitted to the Birch-Murnaghan equation of state (B-M EoS). For the Fe-free CF phase, the fit using a third-order B-M EoS yields the following: unit-cell volume at zero pressure $V_0 = 241(1) \text{ \AA}^3$, isothermal bulk modulus $K_{\text{T0}} = 201(9)$ GPa, and its pressure derivative $K_{\text{T0}}' = 4.2(4)$, and the fit using a second-order B-M EoS yields $K_{\text{T0}} = 204(7)$ GPa with a fixed $K_{\text{T0}}' = 4$. The P - V data of the HS state Fe-bearing CF phase up to 25 GPa (before the abnormal volume reduction) are fitted to a second-order B-M EoS, yielding $V_{0\text{-HS}} = 242.8(2) \text{ \AA}^3$ and $K_{\text{T0-HS}} = 208(3)$ GPa with a fixed $K_{\text{T0}}' = 4$. The P - V data between 42 and 78 GPa for the LS state Fe-bearing CF phase are fitted with a second-order B-M EoS, yielding $V_{0\text{-LS}} = 239(1) \text{ \AA}^3$ and $K_{\text{T0-LS}} = 202(7)$ GPa with a fixed $K_{\text{T0}}' = 4$. The derived V_0 , K_{T0} , and K_{T0}' of the Fe-bearing CF phase for both HS and LS states are in good agreement with those of the Fe-free CF phase, indicating that substitution of 13 mol % iron in aluminum causes an increase of unit-cell volume but has no significant effect on EoS parameters. These derived EoS parameters of both the Fe-free and Fe-bearing CF phases are consistent with values from previous studies [Guignot and Andrault, 2004; Imada et al., 2012]. Using the obtained EoS parameters of the Fe-bearing CF phase, the LS fraction (n_{LS}) can be derived following the thermodynamic methods described previously [Wentzcovitch et al., 2009; Wu et al., 2016a]. As shown in Figure S4, the Fe^{3+} spin transition in the Fe-bearing CF phase starts at ~ 27 GPa and finishes at ~ 42 GPa.

To investigate the effects of Fe^{3+} spin transition on axial compressibility of the CF phase, lattice parameters (a , b , and c) of both Fe-free and Fe-bearing CF phases are plotted in Figure 4. There is no noticeable discontinuity in the P - a , P - b , and P - c curves of the Fe-free CF phase up to 78 GPa. For the Fe-bearing CF phase, axial lengths of the b and c axes decrease smoothly with increasing pressure (Figures 4b and 4c), but the P - a curve exhibits an anomalous reduction in the spin transition zone of octahedral Fe^{3+} (Figure 4a). Further, axial length differences (Δa , Δb , and Δc) between the Fe-bearing and Fe-free CF phases are shown in Figure 4d. The derived P - Δa data show a dramatic reduction of $\sim 0.15 \text{ \AA}$ in the spin transition zone, while no discontinuity is observed for Δb and Δc . Thus, the volume anomaly of the Fe-bearing CF phase in the spin transition zone results almost entirely from a shortening of the a axis. This behavior of the CF phase is similar to that of the NAL phase because of their similar structures [Wu et al., 2016a]. The AlO_6 , SiO_6 , or Fe^{3+}O_6 octahedra of the CF phase

3.3. Equation of State and Axial Compressibility of the CF Phase

The refined lattice parameters of Fe-free and Fe-bearing CF phases at different pressures are listed in Tables S5 and S6 and plotted in Figures 3 and 4. The unit-cell volume of the Fe-free CF phase monotonously decreases with increasing pressure, while for the Fe-bearing CF phase there is a noticeable volume reduction of $\sim 4.5 \text{ \AA}^3$ ($\sim 2.0\%$) at ~ 30 GPa (Figure 3). The pressure region of the abnormal volume reduction coincides with the spin transition zone of octahedral Fe^{3+} as supported by NFS measurements. Thus, the volume discontinuity can be attributed to the HS-to-LS transition of octahedral Fe^{3+} in the CF phase. To identify the onset pressure for the LS state (P_{LS})

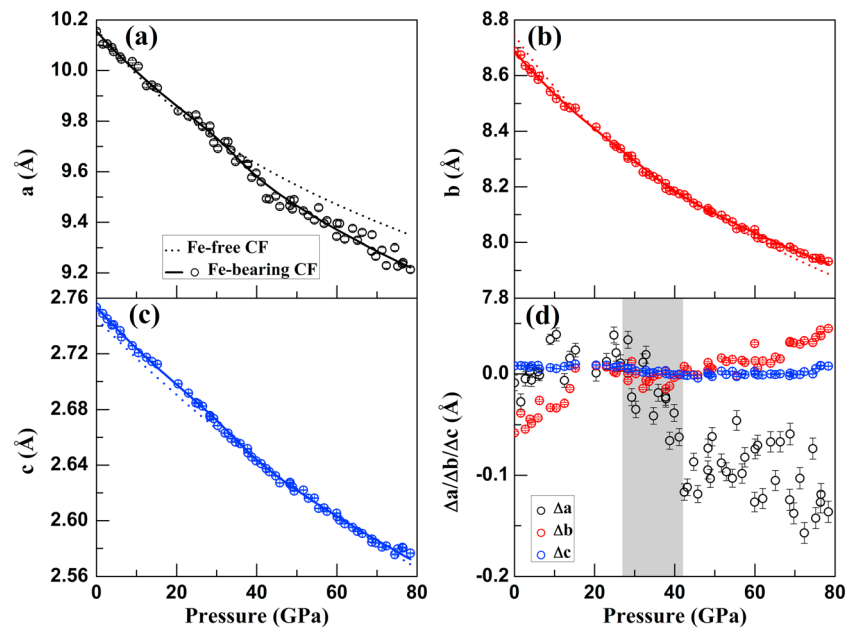


Figure 4. (a–c) Lattice parameters, a , b , and c , of Fe-free and Fe-bearing CF phases at high pressure. (d) Axial length differences (Δa , Δb , and Δc) between Fe-bearing and Fe-free CF phases at high pressure. Open symbols: experimental data; solid and dashed lines: modeled results [Xia *et al.*, 1998; Wentzcovitch *et al.*, 2009]. The gray shaded region represents the spin transition zone of octahedral Fe^{3+} .

are linked by shared edges to form chains parallel to the c axis, and adjacent chains share edges and corners to form large tunnels occupied by Na^+ and Fe^{2+} [Yamada *et al.*, 1983] (Figure S1). Thus, the c axis direction with its stiff chains shows greater resistance to compression compared to the a or b axes direction with their large tunnel spaces.

We observe that only octahedral Fe^{3+} in both NAL and CF phases undergoes a pressure-induced spin transition up to 80 GPa in this study and our previous studies. The CF sample is Mg deficient while the NAL sample has a composition similar to the one expected in the lower mantle [Walter *et al.*, 2011; Wu *et al.*, 2016a] (Table S2), but since octahedral Fe^{3+} is more sensitive to the applied pressure than Fe^{2+} or Fe^{3+} with trigonal prismatic coordination in both NAL and CF phases, the iron spin transition may depend primarily on their crystal structures rather than their Mg and Na contents. We therefore expect the magnitude of the volume and elastic anomalies arising from the spin transition to be related to the amount of octahedral Fe^{3+} ; hence, we consider the results from our studies to be relevant for lower mantle compositions.

4. Geophysical Implications

Thermoelastic properties of deep-subducted MORB are important for inferring the origin of the heterogeneity in the lower mantle. According to the model of subducted slabs from Ringwood [1982] and Irifune [1993], slabs sinking into the lower mantle contain mainly basaltic crust and harzburgite. Depleted pyrolite in the lower layer is stripped off during subduction and resorbed into the upper mantle, while harzburgite has a similar chemical composition, mineral assemblage, and thus density and velocity as pyrolite. Basalt is thus a possible candidate for the observed seismic scatterers or reflectors in the Earth's interior, which have been reported via analysis of scattered seismic waves around circum-Pacific regions in the whole lower mantle [Kaneshima, 2016]. For example, the strong and sharp seismic anomalies beneath the Mariana and Tonga trenches at depths of 1500–1600 km may be attributed to the second-order phase transition from stishovite to $CaCl_2$ -type SiO_2 in subducted basalt [Carpenter *et al.*, 2000; Kaneshima and Helffrich, 2003, 2010; Yang and Wu, 2014]. In addition, many small-scale seismic scatterers observed in the lower mantle may result from other factors which can cause elastic anomalies [Korenaga, 2015; Li and Yuen, 2014; Niu, 2014; Rost *et al.*, 2008; Yang and He, 2015]. These factors include the existence of fluid [Ohtani and Litasov, 2006], hollandite

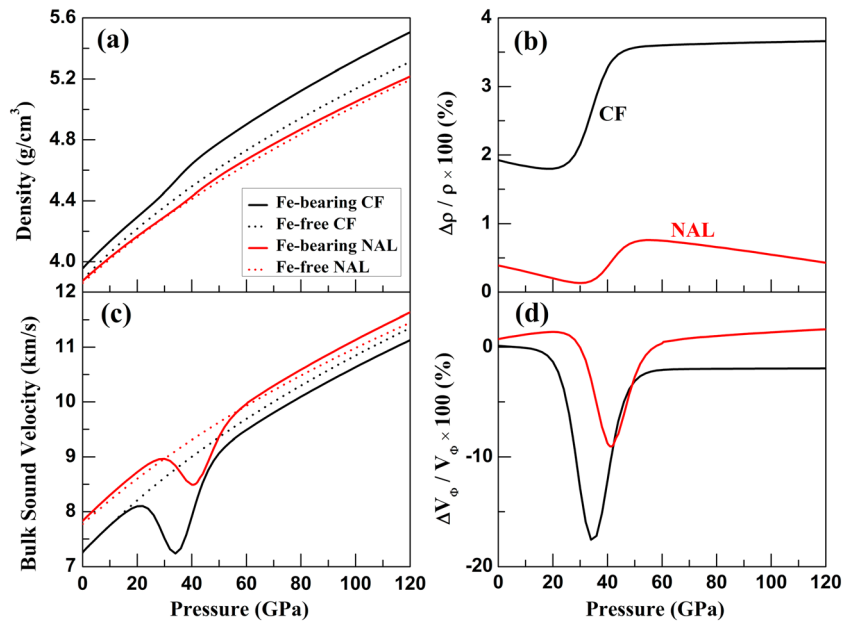


Figure 5. (a) Density and (c) bulk sound velocity profiles of Fe-free and Fe-bearing CF phases at high pressures. The differences of (b) density $(\rho_{\text{Fe-bearing}} - \rho_{\text{Fe-free}}) / \rho_{\text{Fe-free}} \times 100\%$ and (d) bulk sound velocity $(V_{\phi-\text{Fe-bearing}} - V_{\phi-\text{Fe-free}}) / V_{\phi-\text{Fe-free}} \times 100\%$. Density and bulk sound velocity profiles of Fe-free and Fe-bearing NAL phases are also plotted for comparison [Wu et al., 2016a].

[Mookherjee and Steinle-Neumann, 2009], hydrous phase D [X. Wu et al., 2016], and the Al-rich phases [Wu et al., 2016a] in subducted basalt.

To evaluate the effect of the Fe^{3+} spin transition on the elastic properties of subducted MORB in the lower mantle, the bulk sound velocity (V_{ϕ}) for MORB was modeled in our previous study on the NAL phase [Wu et al., 2016a]. The spin transition of octahedral Fe^{3+} in the NAL phase results in a softening of V_{ϕ} for MORB with a maximum reduction of 1.8% at approximately 41 GPa. Results from this study indicate that density (ρ) of the Fe-bearing CF phase increases by $\sim 1.7\%$ and the bulk sound velocity displays a significant reduction up to $\sim 17.6\%$ in the spin transition zone at room temperature (Figure 5). Recently, first-principles calculations predicted that the spin transition pressure of the Fe-bearing NAL phase increases negligibly with temperature while the degree of velocity softening distinctly decreases [Hsu, 2017]. Temperature effects on the spin transition of the CF phase are assumed to be similar to those of the NAL phase due to their similar structures and spin transition behaviors. Thermoelastic properties of subducted MORB can be modeled using our results and the thermoelastic parameters from previous studies (Table S7).

We have modeled density and bulk sound velocity profiles of MORB composition at 300 K and 1200 K across the spin transition zones of NAL and CF phases. Subducted MORB in the lower mantle is assumed to contain 40% bridgmanite [Boffa Ballaran et al., 2012; Katsura et al., 2009], 20% CaSiO_3 perovskite [Li et al., 2006], 20% stishovite or CaCl_2 -type SiO_2 [Andrault et al., 2003; Nishihara et al., 2005], 10% NAL [Shinmei et al., 2005; Wu et al., 2016a], and 10% CF [Sueda et al., 2009] by volume, and the proportions of minerals are assumed to remain constant with depth [Ricolleau et al., 2010] (Table S7). V_{ϕ} profiles of MORB-1 were calculated without considering Fe^{3+} spin transitions in the NAL and CF phases, while V_{ϕ} profiles of MORB-2 were modeled using constituent minerals including the Fe-bearing NAL and CF phases. As shown in Figure 6, densities of either MORB-1 or MORB-2 at 300 K and 1200 K are higher than that of preliminary reference Earth model (PREM) by ~ 0.23 and $\sim 0.15 \text{ g/cm}^3$, respectively [Dziewonski and Anderson, 1981]. In view of the Fe^{3+} spin transition in NAL and CF phases, densities of MORB-2 at 300 K and 1200 K both increase by $\sim 0.24\%$ (Figures 6a and 6b). The bulk sound velocity of MORB-1 at 300 K and 1200 K is higher than that of PREM by 0.1–1 km/s at lower mantle pressures. In comparison with MORB-1, MORB-2 at 300 K exhibits a distinct V_{ϕ} softening at 25–60 GPa up to $\sim 2.3\%$ at ~ 38 GPa. The V_{ϕ} softening region expands and moves to 30–75 GPa at 1200 K, and the maximum of the V_{ϕ} reduction decreases to $\sim 1.8\%$ at ~ 50 GPa (Figures 6c and 6d).

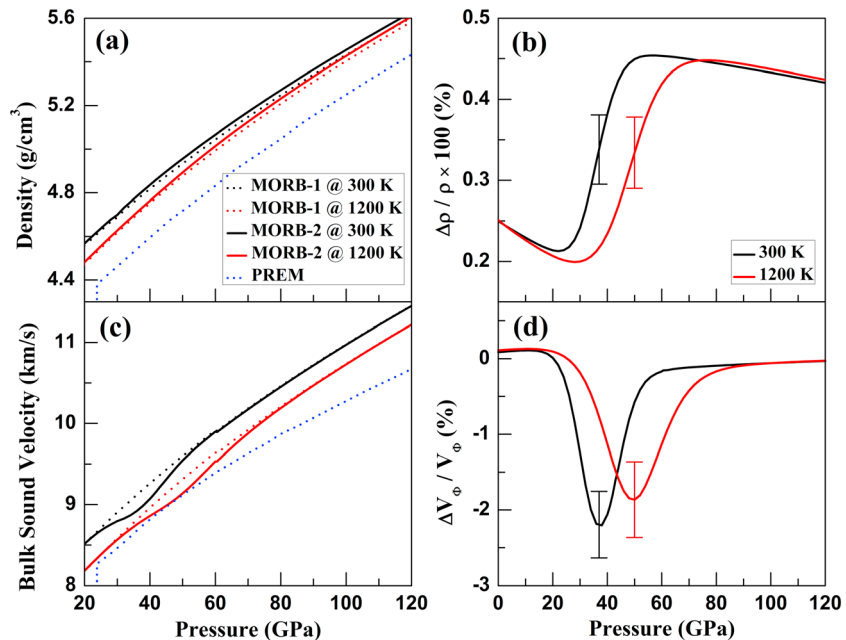


Figure 6. (a) Density and (c) bulk sound velocity profiles of subducted MORB at 300 K and 1200 K. The differences of (b) density ($(\rho_{\text{MORB-2}} - \rho_{\text{MORB-1}}) / \rho_{\text{MORB-1}} \times 100\%$) and (d) bulk sound velocity ($(V_{\phi\text{-MORB-2}} - V_{\phi\text{-MORB-1}}) / V_{\phi\text{-MORB-1}} \times 100\%$). Subducted MORB in the lower mantle is assumed to contain 40% bridgmanite, 20% CaSiO_3 perovskite, 20% stishovite or CaCl_2 -type SiO_2 , 10% NAL, and 10% CF by volume [Ricolleau *et al.*, 2010]. V_{ϕ} profiles of MORB-1 were calculated using constituent minerals including the Fe-free NAL and CF phases, while V_{ϕ} profiles of MORB-2 were modeled considering the Fe^{3+} spin transition in the Fe-bearing NAL and CF phases. The density and V_{ϕ} profiles of PREM are plotted for comparison [Dziewonski and Anderson, 1981].

Synthesis of a CF phase with composition closer to that expected in the lower mantle could be carried out in a future study, although higher pressures would be needed according to the phase diagram of the NaAlSiO_4 - MgAl_2O_4 system [Imada *et al.*, 2011; Ono *et al.*, 2009]. High P - T experiments monitoring iron spin crossover in the NAL and CF phases would provide more accurate data to evaluate their contributions to the thermoelastic properties of subducted MORB in the lower mantle. Based on the results of this study, however, it is clear that Fe^{3+} spin transition in the NAL and CF phases does affect the thermoelastic properties of subducted MORB. The resulting distinct elastic anomalies should be taken into account to understand seismic signatures in the vicinity of subduction zones in the lower mantle.

Acknowledgments

We thank Renbiao Tao and Emma Bullock for the electron microprobe analysis and Sergey N. Tkachev for loading gas medium. We acknowledge financial support from the National Science Foundation of China (41602036, U1232204, 41473056, and 41322028) and the Fundamental Research Funds for the Central Universities (WUT: 2016VA0079 and 2017VB062). High-pressure experiments were performed at HPCAT and GSECARS of the APS, ANL. HPCAT operation is supported by DOE-NNSA under award DE-NA0001974, with partial instrumentation funding by NSF. GSECARS is supported by the NSF-Earth Sciences (EAR-1128799) and the DOE-Geosciences (DE-FG02-94ER14466). APS is a U.S. DOE Office of Science User Facility operated for the DOE Office of Science by ANL under contract DE-AC02-06CH11357. Y. X. acknowledges the support of DOE-BES/DMSE under award DE-FG02-99ER45775. Data used in this study are available from Xiang Wu (e-mail: wuxiang@cug.edu.cn) and Ye Wu (e-mail: yew@whut.edu.cn) upon request.

References

- Akaogi, M., Y. Hamada, T. Suzuki, M. Kobayashi, and M. Okada (1999), High pressure transitions in the system MgAl_2O_4 - CaAl_2O_4 : A new hexagonal aluminous phase with implication for the lower mantle, *Phys. Earth Planet. Inter.*, 115, 67–77, doi:10.1016/S0031-9201(99)00076-X.
- Andrault, D., R. J. Angel, J. L. Mosenfelder, and T. Le Bihan (2003), Equation of state of stishovite to lower mantle pressures, *Am. Mineral.*, 88(2–3), 301–307, doi:10.2138/am-2003-2-307.
- Bina, C., and G. Helffrich (2014), Geophysical constraints on mantle composition, in *Treatise on Geochemistry*, edited by H. D. Holland and K. K. Turekian, pp. 41–65, Elsevier, Oxford.
- Boffa Ballaran, T., A. Kurnosov, K. Glazyrin, D. J. Frost, M. Merlini, M. Hanfland, and R. Caracas (2012), Effect of chemistry on the compressibility of silicate perovskite in the lower mantle, *Earth Planet. Sci. Lett.*, 333, 181–190, doi:10.1016/j.epsl.2012.03.029.
- Carpenter, M. A., R. J. Hemley, and H. K. Mao (2000), High-pressure elasticity of stishovite and the $\text{P4}_2/\text{mnm} \rightleftharpoons \text{Pnmm}$ phase transition, *J. Geophys. Res.*, 105, 10,807–10,816, doi:10.1029/1999JB900419.
- Castle, J. C., and R. D. van der Hilst (2003), Searching for seismic scattering off mantle interfaces between 800 km and 2000 km depth, *J. Geophys. Res.*, 108(B2), 2095, doi:10.1029/2001JB000286.
- Dera, P., K. Zhuravlev, V. Prakapenka, M. L. Rivers, G. J. Finkelstein, O. Grubor-Urošević, O. Tschauer, S. M. Clark, and R. T. Downs (2013), High pressure single-crystal micro X-ray diffraction analysis with GSE_ADA/RSV software, *High Pressure Res.*, 33(3), 466–484, doi:10.1080/08957959.2013.806504.
- Dubrovinsky, L. S., N. A. Dubrovinskaya, V. B. Prokopenko, and T. Le Bihan (2002), Equation of state and crystal structure of NaAlSiO_4 with calcium-ferrite type structure in the conditions of the lower mantle, *Int. J. High Pressure Res.*, 22, 495–499, doi:10.1080/08957950212807.
- Dziewonski, A. M., and D. L. Anderson (1981), Preliminary reference Earth model, *Phys. Earth Planet. Inter.*, 25(4), 297–356, doi:10.1016/0031-9201(81)90046-7.

- Fei, Y., A. Ricolleau, M. Frank, K. Mibe, G. Shen, and V. Prakapenka (2007), High-pressure geoscience special feature: Toward an internally consistent pressure scale, *Proc. Natl. Acad. Sci. U.S.A.*, *104*(22), 9182–9186, doi:10.1073/pnas.0609013104.
- Fukao, Y., and M. Obayashi (2013), Subducted slabs stagnant above, penetrating through, and trapped below the 660 km discontinuity, *J. Geophys. Res. Solid Earth*, *118*, 5920–5938, doi:10.1002/2013JB010466.
- Fukao, Y., M. Obayashi, and T. Nakakuki (2009), Stagnant slab: A review, *Annu. Rev. Earth Planet. Sci.*, *37*, 19–46, doi:10.1146/annurev.earth.36.031207.124224.
- Funamori, N., R. Jeanloz, N. Miyajima, and K. Fujino (2000), Mineral assemblages of basalt in the lower mantle, *J. Geophys. Res.*, *105*(B11), 26,037–26,043, doi:10.1029/2000JB900252.
- Green, D., W. Hibberson, and A. Jaques (1979), Petrogenesis of mid-ocean ridge basalts, in *The Earth: Its Origin, Structure and Evolution*, edited by D. H. Green, W. O. Hibberson, and A. L. Jaques, pp. 265–299, Academic Press, London.
- Guignot, N., and D. Andrault (2004), Equations of state of Na–K–Al host phases and implications for MORB density in the lower mantle, *Phys. Earth Planet. Inter.*, *143–144*, 107–128, doi:10.1016/j.pepi.2003.09.014.
- Hirose, K., Y. Fei, Y. Ma, and H.-K. Mao (1999), The fate of subducted basaltic crust in the Earth's lower mantle, *Nature*, *397*, 53–56, doi:10.1038/16225.
- Hirose, K., N. Takafuji, N. Sata, and Y. Ohishi (2005), Phase transition and density of subducted MORB crust in the lower mantle, *Earth Planet. Sci. Lett.*, *237*(1), 239–251, doi:10.1016/j.epsl.2005.06.035.
- Holland, T. J. B., and S. A. T. Redfern (1997), Unit cell refinement from powder diffraction data: The use of regression diagnostics, *Mineral. Mag.*, *61*, 65–77, doi:10.1180/minmag.1997.061.404.07.
- Hsu, H. (2017), First-principles study of iron spin crossover in the new hexagonal aluminous phase, *Phys. Rev. B*, *95*, 020406, doi:10.1103/PhysRevB.95.020406.
- Imada, S., K. Hirose, and Y. Ohishi (2011), Stabilities of NAL and Ca-ferrite-type phases on the join NaAlSiO₄–MgAl₂O₄ at high pressure, *Phys. Chem. Miner.*, *38*(7), 557–560, doi:10.1007/s00269-011-0427-2.
- Imada, S., K. Hirose, T. Komabayashi, T. Suzuki, and Y. Ohishi (2012), Compression of Na_{0.4}Mg_{0.6}Al_{1.6}Si_{0.4}O₄ NAL and Ca-ferrite-type phases, *Phys. Chem. Miner.*, *39*(7), 525–530, doi:10.1007/s00269-012-0508-x.
- Irfune, T. (1993), Phase transformations in the earth's mantle and subducting slabs: Implications for their compositions, seismic velocity and density structures and dynamics, *Island Arc*, *2*(2), 55–71, doi:10.1111/j.1440-1738.1993.tb00074.x.
- Irfune, T., and A. Ringwood (1993), Phase transformations in subducted oceanic crust and buoyancy relationships at depths of 600–800 km in the mantle, *Earth Planet. Sci. Lett.*, *117*(1), 101–110, doi:10.1016/0012-821X(93)90120-X.
- Kaneshima, S. (2013), Lower mantle seismic scatterers below the subducting Tonga slab: Evidence for slab entrainment of transition zone materials, *Phys. Earth Planet. Inter.*, *222*, 35–46, doi:10.1016/j.pepi.2013.07.001.
- Kaneshima, S. (2016), Seismic scatterers in the mid-lower mantle, *Phys. Earth Planet. Inter.*, *257*, 105–114, doi:10.1016/j.pepi.2016.05.004.
- Kaneshima, S., and G. Helffrich (2003), Subparallel dipping heterogeneities in the mid-lower mantle, *J. Geophys. Res.*, *108*(B5), 2272, doi:10.1029/2001JB001596.
- Kaneshima, S., and G. Helffrich (2010), Small scale heterogeneity in the mid-lower mantle beneath the circum-Pacific area, *Phys. Earth Planet. Inter.*, *183*(1), 91–103, doi:10.1016/j.pepi.2010.03.011.
- Katsura, T., S. Yokoshi, K. Kawabe, A. Shatskiy, M. Manthilake, S. Zhai, H. Fukui, H. Hegoda, T. Yoshino, and D. Yamazaki (2009), P-V-T relations of MgSiO₃ perovskite determined by in situ X-ray diffraction using a large-volume high-pressure apparatus, *Geophys. Res. Lett.*, *36*, L01305, doi:10.1029/2008GL035658.
- Kesson, S., J. F. Gerald, and J. Shelley (1994), Mineral chemistry and density of subducted basaltic crust at lower-mantle pressures, *Nature*, *372*, 767–769, doi:10.1038/372767a0.
- Kojitani, H., R. Hisatomi, and M. Akaogi (2007), High-pressure phase relations and crystal chemistry of calcium ferrite-type solid solutions in the system MgAl₂O₄–Mg₂SiO₄, *Am. Mineral.*, *92*, 1112–1118, doi:10.2138/am.2007.2255.
- Korenaga, J. (2015), Constraining the geometries of small-scale heterogeneities: A case study from the Mariana region, *J. Geophys. Res. Solid Earth*, *120*, 7830–7851, doi:10.1002/2015JB012432.
- Li, J., and D. A. Yuen (2014), Mid-mantle heterogeneities associated with Izanagi plate: Implications for regional mantle viscosity, *Earth Planet. Sci. Lett.*, *385*, 137–144, doi:10.1016/j.epsl.2013.10.042.
- Li, L., D. J. Weidner, J. Brodholt, D. Alfe, G. David Price, R. Caracas, and R. Wentzcovitch (2006), Elasticity of CaSiO₃ perovskite at high pressure and high temperature, *Phys. Earth Planet. Inter.*, *155*(3), 249–259, doi:10.1016/j.pepi.2005.12.006.
- Lin, J. F., S. Speziale, Z. Mao, and H. Marquardt (2013), Effects of the electronic spin transitions of iron in lower mantle minerals: Implications for deep mantle geophysics and geochemistry, *Rev. Geophys.*, *51*, 244–275, doi:10.1002/rog.20010.
- Litasov, K., and E. Ohtani (2004), Relationship between Al-bearing phases NAL and CF in the lower mantle, *Geol. Geofiz.*, *45*(11), 1313–1325.
- Lobanov, S. S., H. Hsu, J. F. Lin, T. Yoshino, and A. F. Goncharov (2017), Optical signatures of low spin Fe³⁺ in NAL at high pressure, *J. Geophys. Res. Solid Earth*, *122*, 3565–3573, doi:10.1002/2017JB014134.
- Mao, H. K., J. Xu, and P. M. Bell (1986), Calibration of the ruby pressure gauge to 800 kbar under quasi-hydrostatic conditions, *J. Geophys. Res.*, *91*(B5), 4673–4676, doi:10.1029/JB091iB05p04673.
- Miyajima, N., K. Fujino, N. Funamori, T. Kondo, and T. Yagi (1999), Garnet-perovskite transformation under conditions of the Earth's lower mantle: An analytical transmission electron microscopy study, *Phys. Earth Planet. Inter.*, *116*, 117–131, doi:10.1016/S0031-9201(99)00127-2.
- Miyajima, N., T. Yagi, K. Hirose, T. Kondo, K. Fujino, and M. Hiroyuki (2001), Potential host phase of aluminum and potassium in the Earth's lower mantle, *Am. Mineral.*, *86*, 740–746, doi:10.2138/am-2001-5-614.
- Mookherjee, M., and G. Steinle-Neumann (2009), Detecting deeply subducted crust from the elasticity of hollandite, *Earth Planet. Sci. Lett.*, *288*(3–4), 349–358, doi:10.1016/j.epsl.2009.09.037.
- Nishihara, Y., K. Nakayama, E. Takahashi, T. Iguchi, and K.-i. Funakoshi (2005), P-V-T equation of state of stishovite to the mantle transition zone conditions, *Phys. Chem. Miner.*, *31*(10), 660–670, doi:10.1007/s00269-004-0426-7.
- Niu, F. (2014), Distinct compositional thin layers at mid-mantle depths beneath northeast China revealed by the USArray, *Earth Planet. Sci. Lett.*, *402*, 305–312, doi:10.1016/j.epsl.2013.02.015.
- Niu, F., H. Kawakatsu, and Y. Fukao (2003), Seismic evidence for a chemical heterogeneity in the midmantle: A strong and slightly dipping seismic reflector beneath the Mariana subduction zone, *J. Geophys. Res.*, *108*(B9), 2419, doi:10.1029/2002JB002384.
- Ohtani, E., and K. Litasov (2006), The effect of water on mantle phase transitions, *Rev. Mineral. Geochem.*, *62*(1), 397–420, doi:10.2138/rmg.2006.62.17.
- Ono, S., E. Ito, and T. Katsura (2001), Mineralogy of subducted basaltic crust (MORB) from 25 to 37 GPa, and chemical heterogeneity of the lower mantle, *Earth Planet. Sci. Lett.*, *190*, 57–63, doi:10.1016/S0012-821X(01)00375-2.

- Ono, A., M. Akaogi, H. Kojitani, K. Yamashita, and M. Kobayashi (2009), High-pressure phase relations and thermodynamic properties of hexagonal aluminous phase and calcium-ferrite phase in the systems $\text{NaAlSiO}_4\text{-MgAl}_2\text{O}_4$ and $\text{CaAl}_2\text{O}_4\text{-MgAl}_2\text{O}_4$, *Phys. Earth Planet. Inter.*, *174*(1), 39–49, doi:10.1016/j.pepi.2008.07.028.
- Ricolleau, A., J. P. Perrillat, G. Fiquet, I. Daniel, J. Matas, A. Addad, N. Menguy, H. Cardon, M. Mezouar, and N. Guignot (2010), Phase relations and equation of state of a natural MORB: Implications for the density profile of subducted oceanic crust in the Earth's lower mantle, *J. Geophys. Res.*, *115*, B08202, doi:10.1029/2009JB006709.
- Ringwood, A. E. (1982), Phase transformations and differentiation in subducted lithosphere: Implications for mantle dynamics, basalt petrogenesis, and crustal evolution, *J. Geol.*, *90*(6), 611–643.
- Rost, S., E. J. Garnero, and Q. Williams (2008), Seismic array detection of subducted oceanic crust in the lower mantle, *J. Geophys. Res.*, *113*, B06303, doi:10.1029/2007JB005263.
- Shinmei, T., T. Sanehira, D. Yamazaki, T. Inoue, T. Irifune, K.-i. Funakoshi, and A. Nozawa (2005), High-temperature and high-pressure equation of state for the hexagonal phase in the system $\text{NaAlSiO}_4\text{-MgAl}_2\text{O}_4$, *Phys. Chem. Miner.*, *32*(8–9), 594–602, doi:10.1007/s00269-005-0029-y.
- Sturhahn, W. (2000), CONUSS and PHOENIX: Evaluation of nuclear resonant scattering data, *Hyperfine Interact.*, *125*(1–4), 149–172, doi:10.1023/A:1012681503686.
- Sueda, Y., T. Irifune, T. Sanehira, T. Yagi, N. Nishiyama, T. Kikegawa, and K.-i. Funakoshi (2009), Thermal equation of state of CaFe_2O_4 -type MgAl_2O_4 , *Phys. Earth Planet. Inter.*, *174*, 78–85, doi:10.1016/j.pepi.2008.07.046.
- Sun, S. S. (1982), Chemical composition and origin of the Earth's primitive mantle, *Geochim. Cosmochim. Acta*, *46*(2), 179–192, doi:10.1016/0016-7037(82)90245-9.
- Vinnik, L., M. Kato, and H. Kawakatsu (2001), Search for seismic discontinuities in the lower mantle, *Geophys. J. Int.*, *147*(1), 41–56, doi:10.1046/j.1365-246X.2001.00516.x.
- Walter, M. J., S. C. Kohn, D. Araujo, G. P. Bulanova, C. B. Smith, E. Gaillou, J. Wang, A. Steele, and S. B. Shirey (2011), Deep mantle cycling of oceanic crust: Evidence from diamonds and their mineral inclusions, *Science*, *334*, 54–57, doi:10.1126/science.1209300.
- Wentzcovitch, R. M., J. F. Justo, Z. Wu, C. R. S. da Silva, D. A. Yuen, and D. Kohlstedt (2009), Anomalous compressibility of ferropericlase throughout the iron spin cross-over, *Proc. Natl. Acad. Sci. U.S.A.*, *106*(21), 8447–8452, doi:10.1073/pnas.0812150106.
- Wu, X., Y. Wu, J. F. Lin, J. Liu, Z. Mao, X. Guo, T. Yoshino, C. McCammon, V. B. Prakapenka, and Y. Xiao (2016), Two-stage spin transition of iron in FeAl-bearing phase D at lower mantle, *J. Geophys. Res. Solid Earth*, *121*, 6411–6420, doi:10.1002/2016JB013209.
- Wu, Y., X. Wu, J. F. Lin, C. A. McCammon, Y. Xiao, P. Chow, V. B. Prakapenka, T. Yoshino, S. Zhai, and S. Qin (2016a), Spin transition of ferric iron in the NAL phase: Implications for the seismic heterogeneities of subducted slabs in the lower mantle, *Earth Planet. Sci. Lett.*, *434*, 91–100, doi:10.1016/j.epsl.2015.11.011.
- Wu, Y., J. Yang, X. Wu, M. Song, T. Yoshino, S. Zhai, S. Qin, H. Huang, and J. F. Lin (2016b), Elasticity of single-crystal NAL phase at high pressure: A potential source of the seismic anisotropy in the lower mantle, *J. Geophys. Res. Solid Earth*, *121*, 5696–5707, doi:10.1002/2016JB013136.
- Xia, X., D. J. Weidner, and H. Zhao (1998), Equation of state of brucite: Single-crystal Brillouin spectroscopy study and polycrystalline pressure-volume-temperature measurement, *Am. Mineral.*, *83*, 68–74, doi:10.2138/am-1998-0107.
- Yamada, H., Y. Matsui, and I. Eiji (1983), Crystal-chemical characterization of NaAlSiO_4 with the CaFe_2O_4 structure, *Mineral. Mag.*, *47*, 177–181, doi:10.1180/minmag.1983.047.343.07.
- Yang, R., and Z. Wu (2014), Elastic properties of stishovite and the CaCl_2 -type silica at the mantle temperature and pressure: An ab initio investigation, *Earth Planet. Sci. Lett.*, *404*, 14–21, doi:10.1016/j.epsl.2014.07.020.
- Yang, Z., and X. He (2015), Oceanic crust in the mid-mantle beneath west-central Pacific subduction zones: Evidence from S to P converted waveforms, *Geophys. J. Int.*, *203*(1), 541–547, doi:10.1093/gji/ggv314.
- Zhao, D. P. (2004), Global tomographic images of mantle plumes and subducting slabs: Insight into deep Earth dynamics, *Phys. Earth Planet. Inter.*, *146*(1–2), 3–34, doi:10.1016/j.pepi.2003.07.032.